Novel fluorescent and secreted transcriptional reporters for quantifying activity of the xenobiotic sensor aryl hydrocarbon receptor (AHR)

Séverine A Degrelle, Ioana Ferecatu, Thierry Fournier

▶ **To cite this version:**

Séverine A Degrelle, Ioana Ferecatu, Thierry Fournier. Novel fluorescent and secreted transcriptional reporters for quantifying activity of the xenobiotic sensor aryl hydrocarbon receptor (AHR). Environment International, 2022, 169, pp.107545. ⟨10.1016/j.envint.2022.107545⟩. ⟨hal-04008980⟩

HAL Id: hal-04008980

https://hal.science/hal-04008980v1

Submitted on 28 Feb 2023

HAL is a multi-disciplinary open access archive for the deposit and dissemination of scientific research documents, whether they are published or not. The documents may come from teaching and research institutions in France or abroad, or from public or private research centers.

L'archive ouverte pluridisciplinaire **HAL**, est destinée au dépôt et à la diffusion de documents scientifiques de niveau recherche, publiés ou non, émanant des établissements d'enseignement et de recherche français ou étrangers, des laboratoires publics ou privés.

HAL Authorization

Environment International 169 (2022) 107545

Contents lists available at ScienceDirect

Environment International

journal homepage: www.elsevier.com/locate/envint

Novel fluorescent and secreted transcriptional reporters for quantifying activity of the xenobiotic sensor aryl hydrocarbon receptor (AHR)

Séverine A. Degrelle [a,b,*], Ioana Ferecatu [a], Thierry Fournier [a]

[a] Université Paris Cité, INSERM, UMR-S1139 Physiopathologie et Pharmacotoxicologie Placentaire Humaine, Microbiote pré et post-natal (3PHM), Paris F-75006, France
[b] Inovarion, Paris F-75005, France

ARTICLE INFO

Handling Editor: Adrian Covaci

Keywords:
AHR
XRE
Reporter gene assay
Luciferase
GFP
Benzo[*a*]pyrene
CYP1A1

ABSTRACT

Aryl hydrocarbon receptor (AHR) is a ligand-dependent transcription factor that plays a critical role in diverse biological processes, including xenobiotic metabolism, carcinogenesis, and physiological functions such as regulation of the immune system and cell differentiation. To improve studies of AHR activity, we constructed two new reporter genes: a fluorescent GFP-tagged histone 2B (XRE-H2B-eGFP) and a secreted nanoluciferase (XRE-pNL1.3[secNluc]). Here, we demonstrate how these reporters can be used to monitor AHR activity in different types of cells, including human primary trophoblasts and cell lines, following incubation with a strong AHR ligand, benzo[*a*]pyrene (B[*a*]P), or an AHR inhibitor (CH223191). Compared to vehicle control cells, a significant increase in AHR activity was observed in cells treated with 0.5 and/or 2 μM B[*a*]P and a significant decrease was detected in response to treatment with 3 μM CH223191. These new plasmids have great potential for use in a variety of applications, such as screening for endogenous or exogenous ligands of AHR.

1. Introduction

The aryl hydrocarbon receptor (AHR) is a ligand-dependent transcription factor that is widely expressed in human cells and tissues (Pohjanvirta and Tuomisto, 1994). As a member of the basic helix-loop-helix/Per-Arnt-Sim (bHLH/PAS) family, AHR translocates into the nucleus and heterodimerizes with another bHLH/PAS protein, aryl hydrocarbon nuclear translocator (ARNT), to activate the transcription of its target genes (Crews, 1998; Denison et al., 2002). The AHR/ARNT complex recognizes and binds to a specific DNA sequence known as the xenobiotic response element (XRE), which is situated in the promoter regions of genes. In this way, AHR/ARNT modulates the transcription of target genes including, but not limited to, the members of cytochrome P450 family 1 (*CYP1A1*, *CYP1A2*, *CYP1B1*). AHR has been implicated in numerous biological processes such as xenobiotic metabolism, immune responses, and cell proliferation, differentiation, and apoptosis (Larigot et al., 2018). Moreover, AHR involvement has been described in the pathogenesis of different diseases (see recent reviews (Gargaro et al., 2021; Napolitano et al., 2021)). AHR regulates the response to xenobiotic toxicity from a variety of exogenous environmental contaminants, such as 2,3,7,8-tetrachlorodibenzo-p-dioxin (TCDD, or dioxine), polycyclic aromatic hydrocarbons (PAHs, such as benzo[*a*]pyrene (B[*a*]P)), and halogenated aromatic hydrocarbons (HAHs) (reviewed in (Larigot et al., 2022)). Despite the number and variety of drugs and environmental pollutants that have been linked with AHR signaling, studies in this area have been hindered by the lack of a robust method for quickly assessing AHR-mediated transcriptional activity.

Currently, AHR-mediated transcriptional activity is typically assayed using a classical luciferase (Luc) assay based on the transient transfection of plasmids in cells (human (Vorrink et al., 2014) or rat (Chan et al., 2003)), or stable cell lines such as human HepG2 (Novotna et al., 2011; Satsu et al., 2015; Sekimoto et al., 2007), human HEK293T (Bystriakova et al., 2019), or mouse H1L7.5c3/rat H4L7.5c2 (Brennan et al., 2015). Commercial tools are also available for this purpose, including a specially designed plasmid (#E4121 Promega), lentivirus (#LTLR031 G&P Biosciences), and stable cell lines (#IB06001-32 Indigo Biosciences; #SL-0075-NP Signosis; #ht2l-ahr and #hpgl-ahr InvivoGen). However, for all these assays, cells must be lysed in order to

Abbreviations: AHR, Aryl hydrocarbon receptor; XRE, Xenobiotic response element; B[*a*]P, Benzo[*a*]pyrene; VCT, Villous cytotrophoblast; ST, Syncytiotrophoblast.

* Corresponding author at: Université Paris Cité, INSERM, UMR-S1139 Physiopathologie et Pharmacotoxicologie Placentaire Humaine, Microbiote pré et post-natal (3PHM), Paris F-75006, France.
E-mail addresses: severine.degrelle@inserm.fr, severine.degrelle@inovarion.com (S.A. Degrelle).

https://doi.org/10.1016/j.envint.2022.107545
Received 10 June 2022; Received in revised form 23 September 2022; Accepted 23 September 2022
Available online 24 September 2022
0160-4120/© 2022 Published by Elsevier Ltd. This is an open access article under the CC BY-NC-ND license (http://creativecommons.org/licenses/by-nc-nd/4.0/).

measure Luc expression, which limits the potential applications. For example, studies of reaction kinetics or XRE activation through time must rely on different batches of cells for each time point.

An alternative approach for investigating the activity of AHR is based on GFP fluorescence. These assays typically involve the use of the stably transfected mouse hepatoma cell line Hepa1c1c7 (Nagy et al., 2002) or transgenic animals (medaka (Ng and Gong, 2013) or zebrafish (Xu et al., 2015)).

Although stable cell lines present several advantages—there is no transfection step, and no need for an internal control to normalize transfection efficiency—they cannot reflect the physiology/specificity of all cells. Thus, results obtained from these cells cannot be generalized to all kinds of tissues.

There is therefore a clear and pressing need for new methods for quantifying and monitoring the activity of AHR in any type of cell. In particular, although transcriptional non-secreted Luciferase reporters for AHR do exist, it would be tremendously helpful to have nuclear-localized fluorescent and secreted luciferase reporters that are suitable for live imaging (and cell sorting) or quantification without the need for destructive sampling. Such tools would be complementary to those already available, but would present a particular advantage when the number of cells is limited (primary cultures for example) or for performing a time course. At the end of the assay, cells could then be used for further experiments (e.g., qPCR, immunoblotting).

The current study presents the construction and validation of two novel reporters for use in assaying AHR-mediated transcriptional activity in various cell models. One reporter is based on fluorescence (GFP or mScarlet) while the other utilizes a secreted luciferase (secNLuc). To evaluate the responses of these reporters, we used a well-characterized and strong agonist of AHR, benzo[*a*]pyrene (B[*a*]P), as well as the well-known inhibitor CH223191. Experiments were carried out in primary human cytotrophoblasts, in which two target genes of AHR - *CYP1A1* and *CYP1B1* - are upregulated during cell differentiation into syncytiotrophoblasts, as described in earlier work by our group (Wakx et al., 2018). The results described here demonstrate the strong potential of our new reporter genes for use in evaluating AHR ligands in different cells and contexts, in order to retain the real-world specificities of tissues of interest.

2. Materials and methods

2.1. Reagents

The AHR agonist (benzo[*a*]pyrene, #31306), inhibitor (CH223191, #182705), and vehicle (cyclohexane, #28920) were purchased from Sigma-Aldrich.

2.2. Exxxthical statement

Placental tissues were obtained from non-smoking women with uncomplicated pregnancy undergoing normal Cesarean section at the Diaconesses Croix Saint-Simon, Antony, and Montsouris maternity units (Paris, France) with the patients' written informed consent. The protocol for this study was carried out according to the Declaration of Helsinki and approved by the local ethics committee (CPP 2015-mai-13909).

2.3. Plasmid constructs

The plasmids XRE-H2B-eGFP and XRE-pNL1.3[secNLuc] were constructed as described in (Degrelle et al., 2017b). The xenobiotic response element (XRE) sequence was amplified by PCR using the XRE(CYP1A1 promotor)-pGL3 reference plasmid (Morel and Barouki, 1998) and appropriate primers (Table 1). The amplified XRE insert was subcloned by restriction enzyme digestion into the *Kpn*I/*Sac*I sites of the pNL1.3 [secNLuc] plasmid, a secreted NanoLuc® luciferase reporter (Promega Corporation), and the *Ase*I/*Bgl*II sites of the H2B-GFP plasmid (Addgene#11680 (Kanda et al., 1998)). The construction map of the plasmids is shown in Fig. 1.

Table 1
Primers used to amplify DNA fragments by PCR for vector construction, confirmation, and generation of cloned fragments.

Primer name	Sequence
XRE-AseI	GCATTAATGCTTCTGGCACATAGTAGTT
XRE-BglII	GAAGATCTGAGCTCAGCTGGGAAG
pGL3-RV3_F	CTAGCAAAATAGGCTGTCCC
pGL3-GL2_R	CTTTATGTTTTTGGCGTCTTCCA
pH2B-GFP_F	TAACCGTATTACCGCCATGC
pH2B-GFP_R	CTTAGCGCTGGTGTACTTG

Restriction enzyme sites added to primer 5′-ends are underlined.

For co-transfection control, and to ensure compatibility with GFP cell lines, the plasmids CMV-H2B-mScarlet-I and XRE-H2B-mScarlet-I were constructed by restriction enzyme digestion. Briefly, the eGFP sequence was replaced by the mScarlet-I sequence from the pLifeAct_mScarlet-i_N1 plasmid (Addgene #85056 (Bindels et al., 2017)) using the *Bam*HI/*Mfe*I sites.

The integrity of the reporter plasmid sequences was confirmed by DNA sequencing. Plasmid DNA was prepared for transfection using the PureLink Expi Endotoxin-Free Maxi Plasmid Purification Kit (#A312127, Invitrogen) according to the manufacturer's instructions.

All plasmids described in this report - XRE-H2B-eGFP and XRE-pNL1.3[secNluc], as well as CMV-H2B-mScarlet-I and XRE-H2B-mScarlet-I - have been submitted for inclusion in the non-profit plasmid repository Addgene (https://www.addgene.org/) and will be available as Plasmid #182294, Plasmid #182295, Plasmid #182297, and Plasmid #182296, respectively.

2.4. Cell cultures, magnetofection, and treatments

Villous cytotrophoblasts (VCT) were isolated from human term placentas as previously described (Alsat et al., 1991; Buchrieser et al., 2019; Degrelle et al., 2017a; Degrelle et al., 2017b; Frendo et al., 2003; Shoaito et al., 2019). Briefly, fetal membranes were removed and placental tissues were cut into small pieces with scissors. After washes with Ca^{2+}, Mg^{2+}-free Hanks' Balanced Salt Solution (HBSS), the villous tissue was gently removed from the core mesenchyme with forceps. Then, minced tissue (~15 g) was digested at 37 °C for 30 min in a shaking incubator (50–60 rpm) in a filtered trypsin solution that contained 500 mg of trypsin powder (Difco), 250 µl 0.1 M $MgCl_2$, 250 µl 0.1 M $CaCl_2$, 75 µl DNase I (50 U/mL) and 10 ml of fat-free milk in 250 ml warm 1X Ca^{2+}, Mg^{2+}-free HBSS. The tissues were then digested again for 10 min, up to 4 or 5 times, at 37 °C with soft shaking (50–60 rpm). Enzymatic degradation was monitored under microscope and stopped by filtering the mixture through a 40-µm strainer (Thermo Fisher Scientific) into fetal calf serum (FCS, 5 % final concentration). After centrifugation of cell suspensions at 1,200 rpm for 10 min at room temperature, cell pellets were resuspended in DMEM, layered on top of a preformed Percoll gradient (60 % and 30 %), and centrifuged at 2,500 rpm at room temperature without braking for 20 min. The interface layer (60 / 30 %) containing villous cytotrophoblast cells was collected, washed in DMEM, and centrifuged at 1200 rpm at room temperature for 10 min. The cell pellet was resuspended in complete culture medium (1 % glutamine and 10 % FCS in DMEM). Cells were counted using a TC20™ Automated Cell Counter (Biorad), and seeded either into a sterile 12-well removable chamber placed on cell culture–treated plastic slides (75,000/well, Ibidi #81201) for fluorescence experiments (immunofluorescence and XRE-H2B-eGFP transfection), or into a sterile 12-well plate (500,000/well, Corning #3512) for nanoluciferase assays (XRE-pNL1.3 transfection) and western blot experiments.

NIH/3T3 (ATCC #CRL-1658) and BeWo (ATCC #CCL-98) cells were cultured in complete high glucose DMEM (1 % glutamine and 10 % FCS) and F12K (1 % glutamine and 10 % FCS), respectively. The cells were

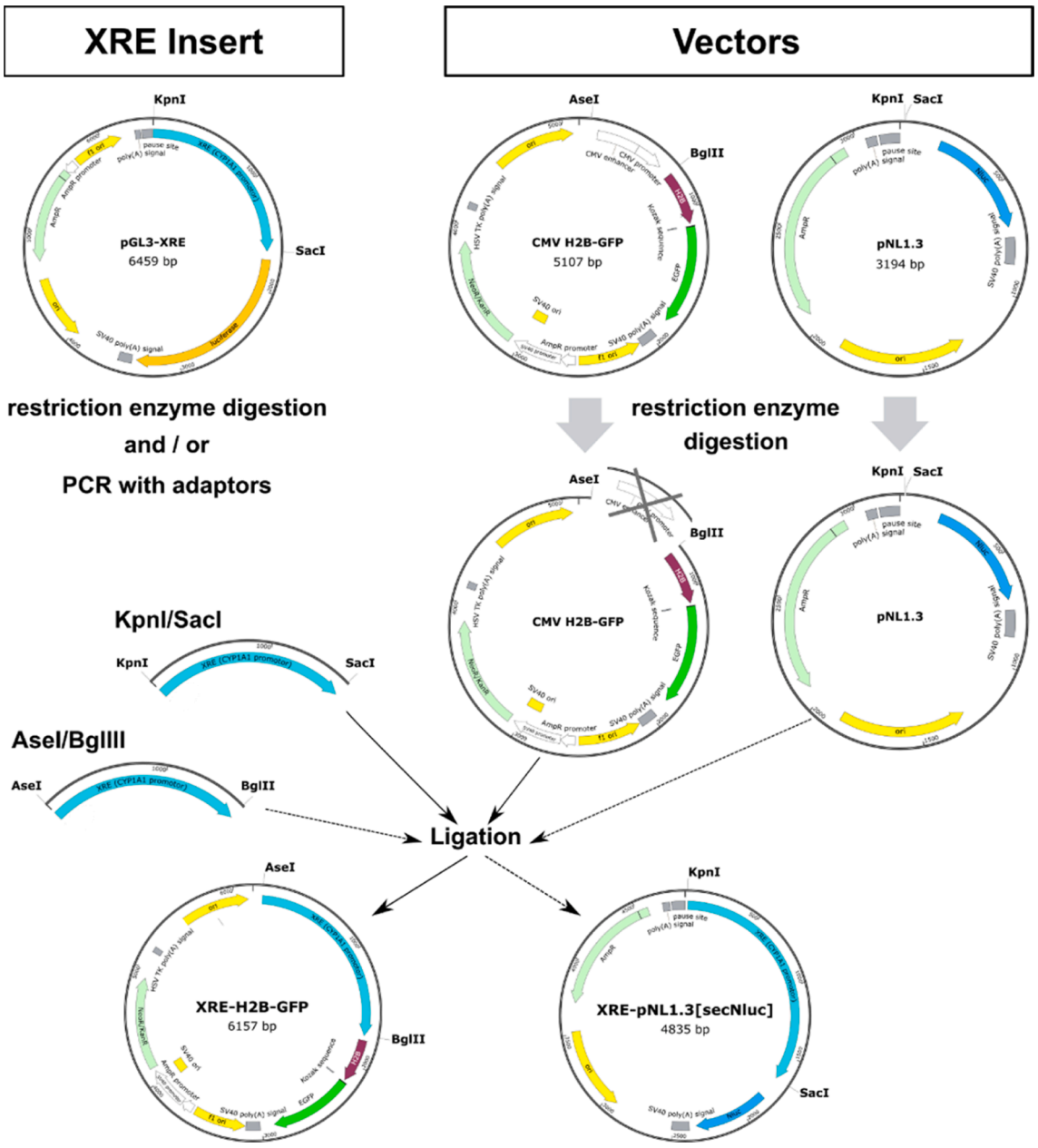

Fig. 1. Schematic diagram of XRE-H2B-eGFP and XRE-pNL1.3[secNLuc] plasmid construction.

seeded in triplets onto either a sterile 12-well plate (125,000/well [NIH/3T3], 250,000/well [BeWo], Corning #3512) for nanoluciferase assays (XRE-pNL1.3 transfection) and western blot experiments or into a sterile 12-well removable chamber placed on cell culture–treated plastic slides (15,000/well [NIH/3T3], 25,000/well [BeWo], Ibidi #81201) for fluorescence experiments (immunofluorescence and XRE-H2B-eGFP transfection).

Cells were transfected as described in (Buchrieser et al., 2019; Shoaito et al., 2020). Briefly, the transfection complexes were composed of Opti-MEM medium mixed with Lipofectamine 2000CD (Invitrogen), Magnetofection CombiMag (OZ Biosciences), and XRE-pNL1.3 [secNLuc] or empty-pNL1.3/CMV-ss.mCherry for nanoluciferase assays or XRE-H2B-GFP/CMV-H2B-mScarlet-I for immunofluorescence. The mixture was incubated for 20 min at room temperature and then distributed into the wells (75 µl/well in the 12-well plate, 30 µl/well in the 12-well slide). Culture plates and slides were placed on a magnetic plate (OZ Biosciences) for at least 10 min at 37 °C and 5 % CO_2, then transferred back into the incubator. After overnight incubation, cells were washed and treated with 0.5 or 2 µM B[*a*]P or 3 µM CH223191 for 24 h.

2.5. Nanoluciferase assay

Cells transfected with XRE-pNL1.3 or empty-pNL1.3/CMV-ss.mCherry were cultured in a 12-well plate for 24 h at 37 °C. Then, cells were treated for 24 h with either 2 µM B[*a*]P (AHR agonist) or 3 µM CH223191 (AHR inhibitor). After treatment, 75 µl of each supernatant was dispensed in duplicate into a 96-well plate (#3610, Corning). The activity of the secreted luciferase was assayed using the Nano-Glo® Luciferase Assay (#N1130 Promega Corporation) according to the manufacturer's instructions. Luminescence and fluorescence of mCherry (Ex: 587 nm, Em: 610 nm) were measured using an EnSpire Multimode plate reader (Perkin Elmer). Each luminescence measurement was standardized to its corresponding mCherry signal and then to the empty-pNL1.3–transfected cells.

2.6. Immunofluorescence and image analysis

After 24 h of treatment with either 0.5 or 2 μM B[*a*]P (AHR agonist) or 3 μM CH223191 (AHR inhibitor), cells were fixed in 4 % PFA for 20 min at room temperature, washed in PBS, and permeabilized in 0.5 % Triton X-100/5 % IgG free BSA/0.1 % Tween-20 in PBS (PBST) for 30 min at room temperature. Then, cells were incubated with primary antibodies: AHR (#WH0000196M2, Sigma, 1:500), CYP1A1 (#13241–1-AP, Proteintech, 1:100), and DSP (#ab71690, Abcam, 1:500) in 5 % IgG free BSA/PBST solution. After overnight incubation at 4 °C, cells were washed with PBST (three times), and incubated with an appropriate secondary antibody or phalloidin coupled with Alexa Fluor 488, 555, or 647 (Invitrogen, 1:500 in PBST) for 1 h, at room temperature in the dark. After washes in PBST (three times), cells were counterstained with DAPI for 10 min at room temperature. Finally, slides were mounted with Fluorescent Mounting Medium (#S3023, Dako) and stored at 4 °C. Confocal microscopy images were obtained with a Leica SP8 inverted microscope equipped with Plan Apo x40/1.3 and x60/1.4 oil objectives; images were processed with ImageJ version 1.52i (National Institutes of Health, https-//imagej.nih.gov/ij/). Quantification of XRE-H2B-eGFP was performed on a minimum of 50 nuclei per condition in three independent experiments. The fluorescent signals were integrated over the entire nucleus as described in (Degrelle et al., 2017b).

2.7. Western blotting

After the nanoluciferase assay on cell supernatants, total cell extracts were lysed using RIPA buffer containing freshly added protease and phosphatase inhibitors (#539131, #524629, Calbiochem), and then sonicated. After centrifugation at 14,000 g at 4 °C for 10 min, protein supernatants were transferred to a new tube. Protein concentrations were determined using the micro BCA™ Protein Assay Kit (#23135, Thermo Scientific). Then, 30 μg of protein samples were separated under reducing conditions on 4–15 % SDS-PAGE mini-PROTEAN® TGX™ gel. After transferring onto a 0.2-μm nitrocellulose membrane using a trans-blot® Turbo™ Transfer System (Bio-rad), membranes were first blocked with 3 % BSA/TBS at room temperature for 1 h, and then, immunoblotted with antibodies to CYP1A1 (1 μg/ml, #13241-1-AP, Proteintech) and Vinculin (1 μg/ml, #V9131, Sigma-Aldrich) in blocking solution at 4 °C overnight. After three washes with 0.1 % Tween-20 in TBS (TBST), the membranes were incubated with an appropriate Alexa Fluor–conjugated secondary antibody (680 or 800 conjugate, Molecular Probes, 1:20,000) at room temperature for 1 h. Finally, after three washes with TBST, the membranes were scanned with an Odyssey® Imaging System (Li-Cor). The quantification of the signal intensity was performed using Image Studio Lite software, version 5.2. For each protein, the arbitrary pixel densities were normalized to those of vinculin.

2.8. Statistics

All measurements were performed at least in three independent experiments. Data are expressed as the mean ± SD of the indicated value. Statistical analysis (one-way ANOVA) was performed using GraphPad Prism 9 version 3.1. Results were considered significant if the p-value was less than 0.05.

3. Results

3.1. AHR and CYP1A1 expression in villous cytotrophoblasts (VCT) and syncytiotrophoblasts (ST)

Before evaluating our two novel AHR reporters, we first used immunostaining to validate AHR expression and the induction of expression of CYP1A1, the main target of AHR, in primary human cytotrophoblasts (Fig. 2A-B). Unlike in our previous study (Wakx et al., 2018), the B[*a*]P used in this study was dissolved in cyclohexane and not in DMSO. It was thus important to validate basal AHR expression and induction of CYP1A1 expression after B[*a*]P/cyclohexane treatment before proceeding with further investigation. Consistent with our previous results (Wakx et al., 2018), we found that AHR is localized in the nuclei of both mononucleated VCT and multinucleated ST (Fig. 2A). The observed expression of CYP1A1 increased in cells treated with the AHR agonist (0.5 μM or 2 μM B[*a*]P) and decreased in cells treated with the AHR inhibitor (3 μM CH223191) (Fig. 2B).

3.2. XRE-H2B-eGFP transfection of VCT - a new fluorescent model for monitoring AHR activity

For the assay, primary cytotrophoblasts were transiently transfected with the novel plasmid XRE-H2B-eGFP, which was combined with the CMV-H2B-mScarlet-I plasmid as a transfection control (Fig. 2C left panel). Co-transfected VCTs (H2B-mScarlet positive nuclei) showed eGFP-positive nuclei whose fluorescence intensity reflected the level of AHR transcriptional activity (Fig. 2C middle panel). Compared to control (vehicle only) cells, this activity (green fluorescence) increased in the cells treated with 0.5 μM or 2 μM B[*a*]P (AHR agonist), and decreased in cells treated with 3 μM CH223191 (AHR inhibitor). Quantification of the GFP fluorescence signal (Fig. 2C right panel) revealed that, compared to vehicle control cells, a significant and dose-dependent increase in intensity was observed in cells treated with 0.5 μM or 2 μM B[*a*]P (2.0 ± 0.8; 3.8 ± 1.7 versus 1.3 ± 0.4, respectively), whereas a significant decrease was observed in cells treated with 3 μM CH223191 (0.8 ± 0.4 versus 1.3 ± 0.4). These results illustrate that the plasmid XRE-H2B-eGFP is an effective tool for following the activity of AHR using cell-imaging methods.

3.3. XRE-pNL1.3[secNLuc] transfection of VCT - a new model for studying AHR activity directly in cell supernatant

The second approach we used to study AHR activity in primary cytotrophoblasts was to transfect VCTs with the novel XRE-pNL1.3 plasmid combined with a CMV-ss.mCherry transfection control that expresses secreted mCherry (Fig. 2D right panel). In this model, activation of AHR leads to secretion of the nanoluciferase protein into the supernatant of transfected cells. Spectrophotometry readings of 75 μl of supernatant from XRE-pNL1.3–transfected and treated VCTs (Fig. 2D left panel) showed that, compared to vehicle-only control cells, a significant and dose-dependent increase in luminescence intensity was observed in cells treated with 0.5 μM or 2 μM B[*a*]P (1.6 ± 0.1; 2.4 ± 0.7 versus 1.0 ± 0.1, respectively), whereas a significant decrease in luminescence intensity was observed in cells treated with 3 μM CH223191 (0.7 ± 0.1 versus 1.0 ± 0.1). We next used XRE-pNL1.3–transfected and B[*a*]P-treated VCTs to assess expression of the AHR target gene *CYP1A1* by immunoblotting. As expected, CYP1A1 expression was significantly increased, in a dose-dependent manner, in cells treated with 0.5 or 2 μM B[*a*]P (2.5 ± 0.4; 6.3 ± 0.8 versus 1, respectively), and significantly decreased in cells treated with 3 μM CH223191 (0.6 ± 0.1 vs 1). These results reveal that XRE-pNL1.3 is another excellent tool for studying AHR activity directly in the cell supernatant, so that transfected cells can then be used for other experiments such as western blotting (as in the present study).

3.4. XRE-H2B-eGFP and XRE-pNL1.3[secNLuc] systems work effectively in different cell types

To confirm that both novel reporters work with other cell types from different species, we evaluated them in classical NIH/3T3 cells (a mouse embryonic fibroblast cell line; Fig. S1) and BeWo cells (a human placental cell line; Fig. S2), which both express AHR and inducible CYP1A1. Using the same approach, both cell lines were transfected and treated with 2 μM B[*a*]P (AHR agonist) and 3 μM CH223191 (AHR

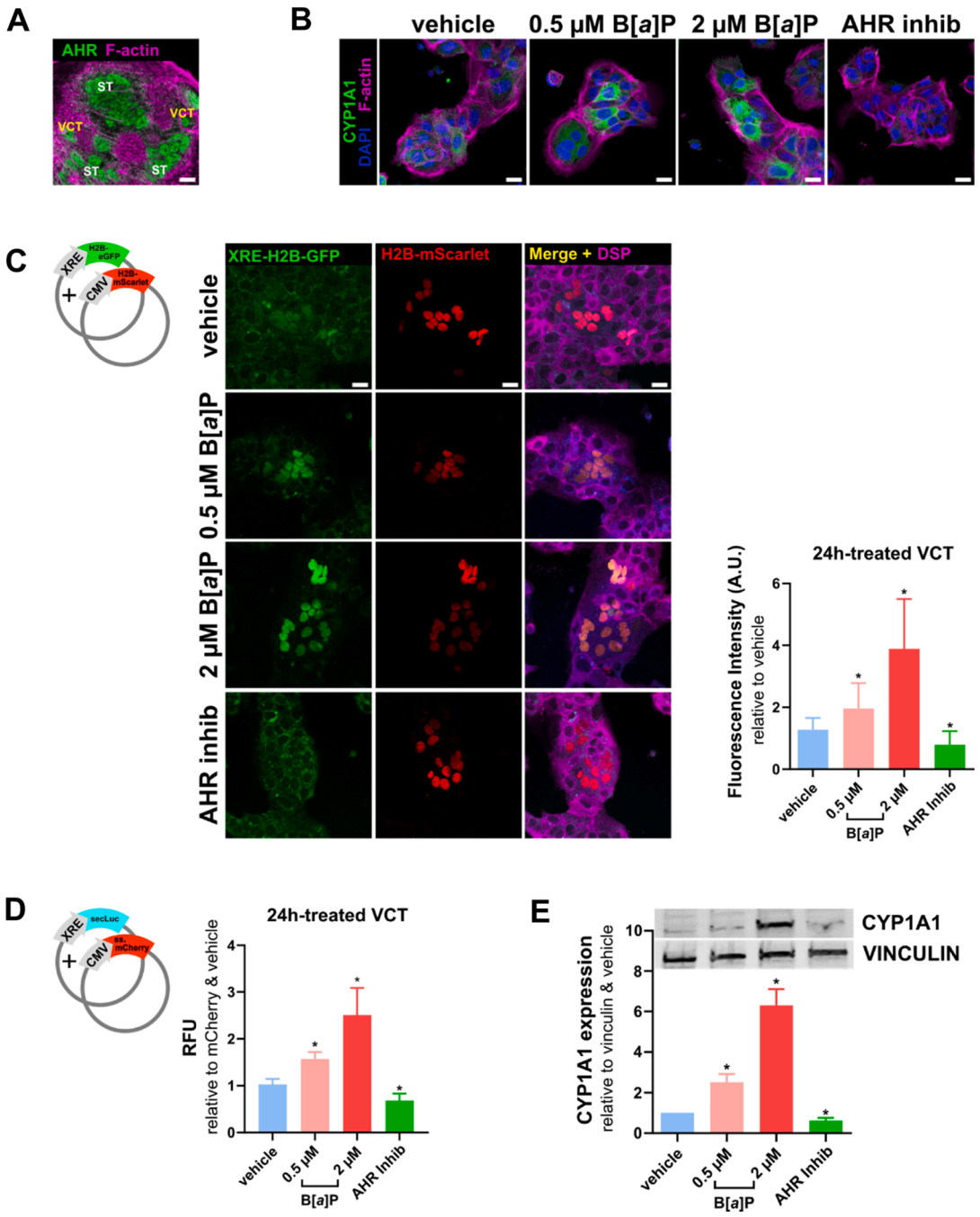

Fig. 2. Visualization and quantification of the activity of AHR using the novel AHR reporters XRE-pNL1.3[secNluc] and XRE-H2B-eGFP in primary human villous cytotrophoblasts (VCT). (A) Localization by immunofluorescence of AHR transcription factor expression in primary VCT/ST after 72 h of culture. AHR nuclear labeling is visualized in green and cell membranes were stained with phalloidin (F-actin, magenta). Scale bar: 20 µm. (B) CYP1A1 protein levels in VCTs assessed using immunofluorescence after 24 h of treatment with either AHR agonist (0.5 µM or 2 µM B[*a*]P) or inhibitor (3 µM CH223191). CYP1A1 labeling is visualized in green; nuclei and cell membranes were stained with DAPI (blue) and phalloidin (F-actin, magenta), respectively. Scale bar: 20 µm. (C) AHR activity evaluated by GFP fluorescence quantification after 24 h of treatment with either AHR agonist (0.5 µM or 2 µM B[*a*]P) or inhibitor (3 µM CH223191) in VCTs co-transfected with XRE-H2B-eGFP (green) and CMV-H2B-mScarlet (red). In the left panel, representative images of co-transfected and treated cells. Cell membranes were immunostained with Desmoplakin (DSP, magenta). Scale bar: 20 µm. In the right panel, quantification of XRE-H2B-eGFP fluorescence intensity performed on H2B-mScarlet + nuclei. Values are represented as mean ± SD normalized with vehicle control (n = 3, > 100 nuclei/experiment). (D) AHR activity assayed using the Nano-Glo® Luciferase system (Promega). For each condition (technical triplicate), 75 µl of culture media were analyzed from VCTs co-transfected with XRE-pNL1.3 and CMV-ss.mCherry after 24 h of treatment with either AHR agonist (0.5 µM or 2 µM B[*a*]P) or inhibitor (3 µM CH223191). Luminescence signal was normalized with the corresponding mCherry signal and vehicle control. Values are represented as mean ± SD (n = 3 independent experiments and with technical triplicates). (E) After the luciferase assay on cell supernatants in (D), cells were harvested and subjected to immunoblot analysis. Representative images are shown of western blots and quantification of CYP1A1 protein level by densitometry using Licor Image Studio Lite software. Values are represented as mean ± SD normalized with vehicle control (n = 3). The asterisk (*) represents a significant difference between vehicle control and treatment [one-way ANOVA, $p < 0.05$]. (For interpretation of the references to colour in this figure legend, the reader is referred to the web version of this article.)

inhibitor). Preliminary results revealed nuclear localization of AHR (Fig. S1A-S2A) and the same CYP1A1 expression patterns as VCTs, i.e. increased expression after B[*a*]P treatment and decreased expression after CH223191 treatment (Fig. S1B-S2B). XRE-H2B-eGFP immunofluorescence data revealed that both cell lines had detectable AHR transcriptional activity in their nuclei with quantifiable GFP fluorescence (Fig. S1C-S2C). As expected, compared to vehicle-only control cells, a significant increase in intensity was observed in cells treated with 2 μM B[*a*]P and a significant decrease was detected in response to treatment with 3 μM CH223191. Transfection with XRE-pNL1.3[secNLuc] confirmed the results regarding AHR activity (Fig. S1D-S2D). CYP1A1 immunoblots on these transfected cells displayed the expected expression profile, i.e. significantly increased or decreased expression after B[*a*]P or CH223191 treatments, respectively (Fig. S1E-S2E).

Finally, to ensure that this tool would also be compatible with a GFP cell line, an XRE-H2B-mScarlet-I plasmid was constructed by replacing the green fluorescent protein (GFP) with a red fluorescent protein (mScarlet-I). We then validated this plasmid in BeWo GFP split cell lines (Buchrieser et al., 2019), a cell fusion model that makes it possible to follow trophoblast differentiation and fusion into a syncytiotrophoblast (Fig. S3).

4. Discussion

In the current paper, we describe the construction and validation of novel XRE gene reporters that enable the measurement of *in vitro* AHR activity. Primary human cytotrophoblasts, murine NIH/3T3, and human BeWo cells were transfected with either fluorescent or nanoluciferase reporters and treated with an AHR activator or inhibitor (B[*a*]P or CH223191, respectively).

Earlier work by our group described the involvement of the AHR pathway in the regulation of *CYP1A1* mRNA expression in human trophoblast cells; specifically, levels of *CYP1A1* increased during the differentiation of VCT into ST, and treating BeWo cells with 1 μM B[*a*]P or 3 μM CH223191 increased or decreased the *CYP1A1* level, respectively (Wakx et al., 2018). In the present study, we confirmed by both immunofluorescence and western blot that levels of CYP1A1 protein follow AHR-pattern activation and are modulated by an activator and inhibitor of AHR in VCT, BeWo, and NIH/3T3 cells. Interestingly, we also observed the nuclear localization of AHR in these three cell types, leading to basal activation of AHR. This could be explained (i) by the presence of kynurenine (200 ng/mg of tissues in term placenta (Murthi et al., 2017)), an endogenous ligand of AHR, (ii) by the presence of ligands from various sources to which pregnant women are unavoidably exposed e.g. through air pollution, dietary exposure, or possibly (iii) by the fetal calf serum used in the culture medium, in which the potent AHR ligands, indirubin and indigo, may have been present (Adachi et al., 2001; Vaziri et al., 1996; Wakx et al., 2018).

In human cytotrophoblasts (VCT), both systems—nuclear fluorescent and secreted nanoluciferase—demonstrated concentration-dependant activation of AHR in response to treatment with two different concentrations of B[*a*]P (0.5 μM or 2 μM).

It is important to note that the three cell types used in this study did not show the same degree of AHR activation following treatment with 2 μM of the agonist B[*a*]P; indeed, the increase in expression was about 4-fold in VCTs, about 2-fold in NIH/3T3s, and only about 1.2-fold in BeWos. This disparity suggests that certain aspects of the AHR activation response are cell line–specific. These observations are consistent with a previous study in which several cell lines (human HepG2, HEK293, and murine HEPA1) were transiently transfected with pGud-Luc1.1 (a plasmid encoding a classical luciferase under the control of four XRE elements) to assess the agonistic effect of different human serum samples on AHR. The authors concluded that AHR activation and signaling could be influenced by cell-specific factors and cell species origin (Rothhammer et al., 2018).

In sum, this work demonstrates the validity and utility of two novel XRE reporter systems for the *in vitro* study of AHR activity. These are complementary existing systems, but possess the major advantages of being compatible with different cell types, including different species, and not requiring cells to be lysed. The secreted nanoluciferase assay described here is highly sensitive, requiring only a small amount of cell supernatant to evaluate changes in luciferase activity. Instead, the fluorescent reporter can be used to monitor AHR activity through live imaging, making it possible to assess reaction kinetics in real time. As an example, this system could be used to perform a time course of AHR activity to assess the cytotoxicity of environmental compounds after just a few hours of exposure. Moreover, these tools can be easily adapted to high-throughput screening of AHR-mediated compounds and natural ligands in any cells or tissues of interest. Our plasmids meet the need for adequate tools for measuring AHR activity in a non-destructive way and enable, for the first time, multiple experiments to be performed with the same batch of cells.

CRediT authorship contribution statement

Séverine A. Degrelle: Conceptualization, Methodology, Investigation, Formal analysis, Visualization, Writing – original draft. **Ioana Ferecatu:** Funding acquisition, Writing – review & editing. **Thierry Fournier:** Resources, Writing – review & editing.

Declaration of Competing Interest

The authors declare that they have no known competing financial interests or personal relationships that could have appeared to influence the work reported in this paper.

Data availability

Data will be made available on request.

Acknowledgments

We are grateful to Xavier Coumoul (INSERM UMR-S1124, T3S, Université de Paris, France) and Julian Buchreiser (CNRS-UMR3569, Institut Pasteur, Paris, France) for providing the XRE-pGL3 plasmid and BeWo GFP split cell lines, respectively. The authors wish to thank the consenting patients and the clinical staff midwives of Diaconesses Croix Saint-Simon, Antony, and Montsouris Hospitals for providing placental tissues, as well as the Cellular and Molecular Imaging facility, UMS3612 CNRS, US25 Inserm, Faculté de Pharmacie de Paris, Université Paris Cité, Paris, France, and Lindsay Higgins for English editing (http://www.englishservicesforscientists.com). This work was supported by ANR (#ANR-20-CE34-0003 PregNanoBaP).

Appendix A. Supplementary data

Supplementary data to this article can be found online at https://doi.org/10.1016/j.envint.2022.107545.

References

Adachi, J., Mori, Y., Matsui, S., Takigami, H., Fujino, J., Kitagawa, H., Miller, C.A., Kato, T., Saeki, K., Matsuda, T., 2001. Indirubin and indigo are potent aryl hydrocarbon receptor ligands present in human urine. J. Biol. Chem. 276 (34), 31475–31478.

Alsat, E., Mirlesse, V., Fondacci, C., Dodeur, M., Evain-brion, D., 1991. Parathyroid hormone increases epidermal growth factor receptors in cultured human trophoblastic cells from early and term placenta. J. Clin. Endocrinol. Metab. 73 (2), 288–295.

Bindels, D.S., Haarbosch, L., van Weeren, L., Postma, M., Wiese, K.E., Mastop, M., Aumonier, S., Gotthard, G., Royant, A., Hink, M.A., Gadella, T.W.J., 2017. mScarlet: a bright monomeric red fluorescent protein for cellular imaging. Nat. Methods 14 (1), 53–56.

Brennan, J.C., He, G., Tsutsumi, T., Zhao, J., Wirth, E., Fulton, M.H., Denison, M.S., 2015. Development of Species-Specific Ah Receptor-Responsive Third Generation

CALUX Cell Lines with Enhanced Responsiveness and Improved Detection Limits. Environ. Sci. Technol. 49 (19), 11903–11912.
Buchrieser, J., Degrelle, S.A., Couderc, T., Nevers, Q., Disson, O., Manet, C., Donahue, D. A., Porrot, F., Hillion, K.-H., Perthame, E., Arroyo, M.V., Souquere, S., Ruigrok, K., Dupressoir, A., Heidmann, T., Montagutelli, X., Fournier, T., Lecuit, M., Schwartz, O., 2019. IFITM proteins inhibit placental syncytiotrophoblast formation and promote fetal demise. Science 365 (6449), 176–180.
Bystriakova, M., Koshkin, S., Tolkunova, E., 2019. Measurement of AhR Ligands in the Tissues of Colon Cancer Patients with XRE Luciferase Reporter. J. Oncol. Res. 1.
Chan, H.Y., Wang, H., Tsang, D.S.C., Chen, Z.-Y., Leung, L.K., 2003. Screening of chemopreventive tea polyphenols against PAH genotoxicity in breast cancer cells by a XRE-luciferase reporter construct. Nutrit. Cancer 46 (1), 93–100.
Crews, S.T., 1998. Control of cell lineage-specific development and transcription by bHLH-PAS proteins. Genes. Dev 12, 607–620.
Degrelle, S.A., Gerbaud, P., Leconte, L., Ferreira, F., Pidoux, G., 2017a. Annexin-A5 organized in 2D-network at the plasmalemma eases human trophoblast fusion. Sci. Rep. 7, 42173.
Degrelle, S.A., Shoaito, H., Fournier, T., 2017b. New transcriptional reporters to quantify and monitor PPARgamma activity. PPAR Res. 2017, 6139107.
Denison, M.S., Pandini, A., Nagy, S.R., Baldwin, E.P., Bonati, L., 2002. Ligand binding and activation of the Ah receptor. Chem. Biol. Interact. 141 (1-2), 3–24.
Frendo, J.L., Cronier, L., Bertin, G., Guibourdenche, J., Vidaud, M., Evain-Brion, D., Malassine, A., 2003. Involvement of connexin 43 in human trophoblast cell fusion and differentiation. J. Cell Sci. 116, 3413–3421.
Gargaro, M., Scalisi, G., Manni, G., Mondanelli, G., Grohmann, U., Fallarino, F., 2021. The Landscape of AhR Regulators and Coregulators to Fine-Tune AhR Functions. Int. J. Mol. Sci 22 (2), 757.
Kanda, T., Sullivan, K.F., Wahl, G.M., 1998. Histone-GFP fusion protein enables sensitive analysis of chromosome dynamics in living mammalian cells. Curr. Biol. 8 (7), 377–385.
Larigot, L., Juricek, L., Dairou, J., Coumoul, X., 2018. AhR signaling pathways and regulatory functions. Biochim. Open 7, 1–9.
Larigot, L., Benoit, L., Koual, M., Tomkiewicz, C., Barouki, R., Coumoul, X., 2022. Aryl Hydrocarbon Receptor and Its Diverse Ligands and Functions: An Exposome Receptor. Annu. Rev. Pharmacol. Toxicol. 62 (1), 383–404.
Morel, Y., Barouki, R., 1998. Down-regulation of cytochrome P450 1A1 gene promoter by oxidative stress. Critical contribution of nuclear factor 1. J. Biol. Chem. 273 (41), 26969–26976.
Murthi, P., Wallace, E.M., Walker, D.W., 2017. Altered placental tryptophan metabolic pathway in human fetal growth restriction. Placenta 52, 62–70.
Nagy, S.R., Sanborn, J.R., Hammock, B.D., Denison, M.S., 2002. Development of a green fluorescent protein-based cell bioassay for the rapid and inexpensive detection and characterization of ah receptor agonists. Toxicol. Sci. 65, 200–210.
Napolitano, M., Fabbrocini, G., Martora, F., Picone, V., Morelli, P., Patruno, C., 2021. Role of aryl hydrocarbon receptor activation in inflammatory chronic skin diseases. Cells 10 (12), 3559.
Ng, G.H.B., Gong, Z., 2013. GFP transgenic medaka (Oryzias latipes) under the inducible cyp1a promoter provide a sensitive and convenient biological indicator for the presence of TCDD and other persistent organic chemicals. PLoS One 8 (5), e64334.
Novotna, A., Pavek, P., Dvorak, Z., 2011. Novel stably transfected gene reporter human hepatoma cell line for assessment of aryl hydrocarbon receptor transcriptional activity: construction and characterization. Environ. Sci. Technol. 45 (23), 10133–10139.
Pohjanvirta, R., Tuomisto, J., 1994. Short-term toxicity of 2,3,7,8-tetrachlorodibenzo-p-dioxin in laboratory animals: effects, mechanisms, and animal models. Pharmacol. Rev. 46, 483–549.
Rothhammer, V., Borucki, D.M., Kenison, J.E., Hewson, P., Wang, Z., Bakshi, R., Sherr, D. H., Quintana, F.J., 2018. Detection of aryl hydrocarbon receptor agonists in human samples. Sci. Rep. 8, 4970.
Satsu, H., Yoshida, K., Mikubo, A., Ogiwara, H., Inakuma, T., Shimizu, M., 2015. Establishment of a stable aryl hydrocarbon receptor-responsive HepG2 cell line. Cytotechnology 67 (4), 621–632.
Sekimoto, M., Kawamagari, H., Nakatani, S., Nemoto, K., Degawa, M., 2007. Establishment of a Human Hepatoma Cell Line HepG2-A10 for a Reporter Gene Assay of Arylhydrocarbon Receptor Activators. Genes. and. Environment 29 (1), 11–16.
Shoaito, H., Petit, J., Chissey, A., Auzeil, N., Guibourdenche, J., Gil, S., Laprevote, O., Fournier, T., Degrelle, S.A., 2019. The Role of Peroxisome Proliferator-Activated Receptor Gamma (PPARgamma) in Mono(2-ethylhexyl) Phthalate (MEHP)-Mediated Cytotrophoblast Differentiation. Environ. Health. Perspect. 127, 27003.
Shoaito, H., Chauveau, S., Gosseaume, C., Bourguet, W., Vigouroux, C., Vatier, C., Pienkowski, C., Fournier, T., Degrelle, S.A., 2020. Peroxisome proliferator-activated receptor gamma-ligand-binding domain mutations associated with familial partial lipodystrophy type 3 disrupt human trophoblast fusion and fibroblast migration. J. Cell. Mol. Med. 24 (13), 7660–7669.
Vaziri, C., Schneider, A., Sherr, D.H., Faller, D.V., 1996. Expression of the aryl hydrocarbon receptor is regulated by serum and mitogenic growth factors in murine 3T3 fibroblasts. J. Biol. Chem. 271 (42), 25921–25927.
Vorrink, S.U., Severson, P.L., Kulak, M.V., Futscher, B.W., Domann, F.E., 2014. Hypoxia perturbs aryl hydrocarbon receptor signaling and CYP1A1 expression induced by PCB 126 in human skin and liver-derived cell lines. Toxicol. Appl. Pharmacol. 274 (3), 408–416.
Wakx, A., Nedder, M., Tomkiewicz-Raulet, C., Dalmasso, J., Chissey, A., Boland, S., Vibert, F., Degrelle, S., Fournier, T., Coumoul, X., Gil, S., Ferecatu, I., 2018. Expression, Localization, and Activity of the Aryl Hydrocarbon Receptor in the Human Placenta. Int. J. Mol. Sci. 19 (12), 3762.
Xu, H., Li, C., Li, Y., Ng, G.H.B., Liu, C., Zhang, X., Gong, Z., 2015. Generation of Tg (cyp1a:gfp) Transgenic Zebrafish for Development of a Convenient and Sensitive In Vivo Assay for Aryl Hydrocarbon Receptor Activity. Mar. Biotechnol. (NY) 17 (6), 831–840.